Reactive tunnel junctions in electrically-driven plasmonic nanorod metamaterials

Pan Wang[#*], **Alexey V. Krasavin**[#], **Mazhar E. Nasir**, **Wayne Dickson**, and **Anatoly V. Zayats**[*]
Department of Physics, King's College London, Strand, London WC2R 2LS, UK

[#] These authors contributed equally to this work.

Abstract

Hot, nonequilibrium carriers formed near the interfaces of semiconductors or metals play a crucial role in chemical catalysis and optoelectronic processes. In addition to optical illumination, an efficient way to generate hot carriers is by excitation with tunnelling electrons. Here we show that the generation of hot electrons makes the nanoscale tunnel junctions highly reactive and facilitates strongly confined chemical reactions which can in turn modulate the tunnelling processes. We designed a device containing an array of electrically-driven plasmonic nanorods with up to 10^{11} tunnelling junctions per square centimeter, which demonstrates hot-electron activation of oxidation and reduction reactions in the junctions, induced by the presence of O_2 and H_2 molecules, respectively. The kinetics of the reactions can be monitored in-situ following the radiative decay of tunnelling-induced surface plasmons. This electrically-driven plasmonic nanorod metamaterial platform can be useful for the development of nanoscale chemical and optoelectronic devices based on electron tunnelling.

Quantum-mechanical tunnelling enables the transport of electrons across a nanoscale gap between two conducting electrodes. The broadband fluctuations in the tunnelling current can excite surface plasmons - the collective oscillations of free electron gas - in metallic nanostructures, providing a method for plasmon excitation with several distinct advantages, including high compactness, fast response, and free of background noise[1–5]. The electron-to-plasmon conversion efficiency is only about one plasmon per 10^5 electrons in metal-dielectric-metal junctions[1,5] and scanning-tunnelling-microscope experiments[2–4]. However, this can be improved by one or two orders of magnitude by nanostructure design (using single optical antennas or their microscale arrays)[6–8]. In addition, assembling such electrically-driven nanoantennas using metamaterial approaches on a macroscopic scale

[*]Correspondence and requests for materials should be addressed to P.W. or A.V.Z. pan.wang@kcl.ac.uk, a.zayats@kcl.ac.uk.

would allow additional flexibility in engineering the local density of optical states, a crucial step to efficient surface plasmon generation.

Optically excited surface plasmons have recently been proposed for the efficient generation of hot carriers[9–11], which can be productively used for chemical catalysis and optoelectronics[9,10,12–17] if extracted from the metal into its surroundings before they thermalize by heat generation[10,18]. During the tunnelling process, the majority of electrons tunnel elastically (maintaining their energy), appearing as energetic hot electrons in the receiving electrode[19]. Therefore, tunnel junctions can be used to harvest hot electrons for the controllable activation of highly-confined chemical reactions. Since tunnelling is extremely sensitive to any changes in the nanometer scale tunnelling gap[20,21], it can be significantly influenced by chemical processes, thus affecting surface plasmon generation due to inelastic tunneling and related light emission. In this manner, tunneling can be used for real-time detection of environmental changes at the molecular level in the junctions, serving as both nanoreactors and sensors, and for the investigation of hot-electron effects.

One prospective metamaterial design to maximally exploit tunnelling effects is an array of electromagnetically coupled nanorods in which each nanorod functions both as a tunnel tip and as an optical antenna (Fig. 1a,b). The typical nanorod areal densities are as high as 10^{10} to 10^{11} cm^{-2}, while the metamaterials can cover macroscopic areas due to the scalable electrochemical fabrication technique. The large surface area provided by this type of metamaterial and the responsiveness to refractive index changes have already been employed for record-sensitivity biological[22] and chemical[23] sensing, ultrasound detection[24] as well as for water splitting[12].

Here, by taking advantage of high-density Au nanorod arrays, we demonstrate the stimulation of hot electrons, surface plasmons and light emission in the metamaterials by electron tunnelling over a macroscopic (up to ~1 cm^2) surface area. The large flux of hot electrons makes the tunnel junctions highly reactive as demonstrated here on the example of strongly confined oxidation and reduction reactions involving O_2 and H_2, respectively. These reactions are monitored either optically by changes in the intensity of light emission (~50%) resulting from the radiative decay of tunnelling-generated surface plasmons, or electrically via tunnelling current variations (~10%).

Design of electrically-driven nanorod metamaterials

Experimentally, the plasmonic nanorod metamaterials were fabricated by direct electrodeposition of Au into substrate-supported porous Al_2O_3 templates (see Methods and Supplementary Section 1). Figure 1c shows the surface morphology of an ion-milled (Supplementary Section 2) metamaterial (nanorod diameter $d \approx 50$ nm, length $l \approx 420$ nm, and separation between the nanorods $s \approx 100$ nm). The nanorod tips are several nanometers lower than the surrounding Al_2O_3 matrix (Supplementary Fig. 1). The optical transmission spectra obtained with TM polarized light (Fig. 1d) are dominated by two nearly-merged polarization-dependent extinction peaks as the metamaterial is strongly anisotropic[25,26]. The reflection spectra reveal the two guided modes supported by the metamaterial slab when illuminated in the attenuated total internal reflection geometry. The counterparts of these

modes also exist within the light cone in the low wave-vector region, corresponding to relatively low quality-factor Fabry-Perot modes26.

Taking advantage of the nanometer-scale height difference between the Au nanorods and the surrounding Al_2O_3 matrix (Fig. 1c), it is straightforward to construct electrically-driven plasmonic nanorod metamaterials based on metal-air-metal tunnel junctions by using liquid eutectic gallium-indium (EGaIn) as a top contact5 (Fig. 2a, see Methods and Supplementary Section 3). When a bias is applied between the Au nanorods and EGaIn, electrons tunnel across the nanometer-scale air gaps from occupied states in EGaIn to unoccupied states in Au nanorods (Fig. 2b). The majority of electrons tunnel elastically, appearing as hot electrons in the Au nanorods. The electrons which tunnel inelastically can excite plasmonic modes in the nanorods forming the metamaterial. The excited plasmons can then either radiate into free-space light via the metamaterial slab modes or decay into hot carriers in the nanorods.

Electric excitation of plasmons in metamaterials

A typical current–voltage curve for the device (Fig. 2c) shows that the measured current increases nonlinearly with the increasing bias, confirming electron tunnelling through the air gaps27. The experimental result is in excellent agreement with numerical simulations of the electron tunnelling process (Fig. 2c, see Supplementary Section 4), in which the averaged thickness of the air gaps was estimated to be around 1.15 nm. Strong light emission of a distinctly red colour (an area of approximately 4 mm^2) was observed from the substrate side when a bias of 2.5 V was applied (inset of Fig. 2c). The observed emission is due to the excitation of a metamaterial plasmonic mode via the inelastic tunneling process, which subsequently radiates into free space (Fig. 2b). Due to the large number of effective nanoscale tunnel junctions in the metamaterial (nanorod areal density approximately 1.3×10^{10} cm^{-2}), the emission is visible to the naked eye, making signal detection trivial for practical applications as well as providing a large surface area comprised of multiple nanorods for the extraction of hot electrons. The efficiency of the inelastic tunnelling process is estimated to be about 0.1% (Supplementary Section 5), a value which qualitatively agrees with previous experimental observations7 and theoretical predictions28,29.

The emission spectra measured under varying forward bias (Fig. 2d and Supplementary Section 6) are relatively broad, typical for tunnelling-based excitation. With an increasing applied bias, the intensity of emission increases gradually (Supplementary Fig. 4), and is accompanied by a blue-shift of the cutoff wavelength. This is expected for light emission generated by inelastic tunnelling electrons1,5–7, as the energies of the emitted photons are always less than the energy of tunnelling electrons (see Methods and Supplementary Section 8). The simulated spectra of the tunnelling-electron-induced emission are in excellent agreement with the experimental observations (Fig. 2e); their shape is defined by the product of the emission spectrum of the tunnelling current source, the modal profile of the metamaterial and the radiation efficiency of the excited modes7 (see Methods). Particularly, the field map of the E_x component of the electric field (Fig. 2f) related to the cylindrical plasmon modes of the nanorods, clearly shows that the maximum emitted intensity (Fig. 2e)

corresponds to the coupling of the tunnelling-excited surface plasmons to the metamaterial mode (mode 3), which facilitates radiation into the far-field measured in the experiment.

Hot-electron-activated reactive tunnel junctions

Considering that the inelastic tunnelling efficiency is estimated to be ~0.1%, approximately 99.9% of the electrons tunnel elastically appearing as hot electrons in the nanorod tips. Under a forward bias of 2.5 V (tunnelling current of ~0.085 A, Fig. 2c), hot electrons are generated at a rate of ~10^9 s^{-1} in the tip of each nanorod with the same energy of 2.5 eV (different from the plasmon-induced hot electrons with broad energy and spatial distributions[30]). The highly efficient and confined hot-electron generation makes the tunnel junctions highly reactive and opens up opportunities for modulating the tunnelling processes via the hot-electron-activated reactions. To demonstrate this capability, we stimulated hot-electron-driven oxidation and reduction reactions involving O_2 and H_2 in the junctions which were monitored in real time by observing the modified light emission from the metamaterial.

To make use of the hot electrons for chemical reactions, metal-polymer-metal tunnel junctions were constructed (Fig. 3a) allowing to access the tunnelling region instead of the closed metal-air-metal tunnel junctions (Fig. 2a). Beginning with a nanorod metamaterial ($d \approx 66$ nm, $l \approx 480$ nm, $s \approx 105$ nm), the Al_2O_3 matrix was first chemically etched in order to expose the Au nanorod tips (Supplementary Section 10), so that they were ~10 nm higher than the surrounding template facilitating the interaction of tunnel junctions with the gas molecules (Fig. 3b). The nanorod tips were then functionalized with a monolayer of poly-L-histidine (PLH) which works both as a tunnel barrier and a reactant (see Methods and Supplementary Section 11), and finally a droplet of EGaIn was added on top. Under an applied bias, a nonlinear current–voltage curve and associated light emission were observed from the device (Supplementary Fig. 8), confirming tunnelling process in the functionalized nanorod tips.

The electrically-driven metamaterial was then placed in a gas cell and both the tunnelling current and the light emission spectrum were monitored simultaneously (Supplementary Section 13). At the beginning, the cell was purged with 2% H_2 in N_2 atmosphere and then maintained in pure N_2. When O_2 was subsequently introduced into the gas cell with air, the emission intensity gradually increased reaching twice the original value (Fig. 3c). Then, following the reintroduction of 2% H_2 in N_2, the light emission intensity decreased back to the initial value (Fig. 3d). By cycling the cell atmosphere between air with 26% relative humidity (RH), N_2, 2% H_2 in N_2, O_2, and 2% H_2 in N_2 with 75% RH (Fig. 3e), it was confirmed that the observed changes of the emission intensity, which reflect the modification of the tunnel junctions, were caused by the reaction of tunnel junctions with O_2 and H_2 molecules (Supplementary Section 14). It is worth noting that it takes several minutes to complete the reactions due to the highly-confined metal-PLH-metal tunnel junctions which hinders the fast diffusion of gas molecules.

We have also investigated the effect of the applied bias on the induced chemical processes. This was conducted by firstly measuring the stabilized emission spectrum characteristic of

the tunnel junctions in an environment of ambient air or 2% H_2 in N_2 at an applied sensing bias of 2.5 V. Then, the bias was varied to a predetermined test value (2.5, 2.0, 1.5, 1.0, 0.5, and 0 V), the cell atmosphere was exchanged, and the device was kept under this bias for 10 minutes. In order to interrogate the tunnel junction state after the test period, the bias was changed back to 2.5 V, and a sequence of emissions spectra were recorded every 50 s until the device reached saturation. Figure 4a shows the percentage change in emission intensity during the 10-min period under different value of test bias (plotted from Supplementary Fig. 10). It was observed that the chemical reactions involving O_2 (blue bars in Fig. 4a) and H_2 (red bars in Fig. 4a) molecules are highly dependent on the applied bias; the higher the bias, the faster the rate of the reaction. The bias-dependent response is highly indicative of the role of the hot-electron energy on the reactions which depends on the voltage applied to the tunnel junction, as was discussed above.

In order to further verify the role of hot electrons in the reactions, we studied the reactions in the unbiased ($V_b = 0$ V, no tunnelling-induced hot electrons) tunnel junctions while under external illumination which can generate hot electrons via the optically excited plasmons (Supplementary Section 15). The response to the reaction with O_2 is highly dependent on the illumination wavelength (blue bars in Fig. 4b and Supplementary Figs. 11a–d). The emission intensity increased 100% to the highest level during the test period when the surface plasmons related to the nanorods forming the metamaterial were efficiently excited (500-750 nm illumination, see inset of Fig. 4b), whereas in the case of less efficient plasmonic excitation (>800 nm illumination), the emission intensity change is almost the same as without illumination. This directly confirms the role of hot electrons in the chemical reaction involving the O_2 molecules: when the device is operated under 2.5 V in N_2, hot electrons are mainly generated in the Au nanorod tips via the elastic tunnelling of electrons[19] (Fig. 2b and process 1 in Fig. 4c); upon the switching of cell atmosphere from N_2 to air, O_2 molecules diffuse into the tunnel junctions and interact with the hot electrons, forming transient negative O_2^- species facilitated via hot-electron transfer from the Au to the antibonding orbital of O_2 and eventually dissociated into O atoms[14,31,32]. The O atoms subsequently form Au oxides with the surface atoms of Au nanorod tips (although Au is the most resistant noble metal to oxidation in air even at elevated temperature, Au oxides can be formed in highly reactive environments[33,34]), while the Au oxides can in turn oxidize the PLH monolayer (NH group in the imidazole rings and/or amino groups of PLH near the nanorod tips can undergo oxidative dehydrogenation and coupling reactions)[14,31,34–36]. The oxidation of the tunnel junctions finally causes a change in the tunnelling barrier that subsequently changes the plasmon excitation and, therefore, the light emission intensity (process 2 in Fig. 4c, optically revealed in Fig. 3c). The reaction induced by H_2 molecules is not influenced by the external illumination (red bars in Fig. 4b and Supplementary Figs. 11e–h). This is due to the formation of Au oxides after reaction in air which can hinder the interaction of plasmon-induced hot electrons with H_2 molecules. And the plasmon-assisted heat generation under the external illumination condition (~0.1 W cm^{-2}) is not enough to activate the reaction of H_2 molecules with the Au oxides. However, in the case of tunnelling (electric power density of ~5.6 W cm^{-2} under an applied bias of 2.5 V), the elevated temperature in the tunnel junctions (~63°C, see Supplementary Section 16), mainly due to the relaxation of the hot electrons[37], can improve the reactivity of H_2 molecules facilitating

the reduction of Au oxides (because of the Arrhenius dependence of rate constants on temperature[38,39]). This subsequently makes the hot electrons accessible, resulting in the dissociation of H_2 molecules into H atoms[13,40] and then the full recovery of the tunnel junctions (hydrogenation of the oxidized PLH monolayer back to PLH) together with the plasmon excitation and light emission (process 3 in Fig. 4c, optically revealed in Fig. 3d). At the same time, metastable gold hydride can form due to the absorption of H atoms on the nanorod tips[31,41] (process 4 in Fig. 4c), evidenced by the emission intensity change when the device was purged with N_2 after the reaction with H_2 molecules (black circles in Fig. 3e). It can be estimated that about 10^{-5} % of the input electric energy is used for the chemical reactions during the reaction period limited by small number of available molecules in the nanojunctions (Supplementary Section 17). The chemical reactions influence both the light emission intensity and the tunnelling current when the cell atmosphere was cycled between air and 2% H_2 (Fig. 4d). The change of the emission intensity exhibits an opposite trend to that of the current, which may be attributed to the difference in the inelastic tunnelling efficiencies through pristine and oxidized tunnel junctions.

The nanoscale reactive tunnel junctions demonstrated above can also be considered for gas sensing. Due to the high spatial confinement of the electron tunnelling process and its extreme sensitivity to the junction properties[20,21,42], as well as the abundant energetic hot electrons in the junctions, it is promising to develop sensors based on electrically-driven plasmonic nanorod metamaterials with atomic level sensitivity and small footprint. As shown in Fig. 4d, the changes in the emission intensity are about 5 times higher than that of the tunneling current (50% vs 10%), indicating the high sensitivity of optical detection for tunnelling-based sensors (the non-optimized sensitivity for H_2 sensing demonstrated here is about two times higher than the previous result based on Pd-coated Au nanorod metamaterials[23]). In addition, by choosing an appropriate material for the functionalization of tunnel junctions, the device can be designed to transduce a variety of chemical and physical stimuli (e.g., gas, molecule, light, or pressure).

Conclusions

We have demonstrated the potential for controlling chemical reactions at the nanoscale using tunnelling-driven generation of hot electrons in metal-polymer-metal gaps. By monitoring either the changes in the tunnelling current or the light intensity due to radiation of the excited plasmonic modes, we have demonstrated both optical and electrical detection schemes that allow for a precise monitoring of the tunnel junction's reactive properties. In addition to the sensing applications, it is evident that the electrically-driven metamaterial platform can also be used as an array of nanoreactors. It can be applied for the *in-situ* studies and real-time monitoring of chemical transformation of molecules functionalized in the junctions, such as the oxidation of aromatic amines or the reduction of aromatic nitro compounds to produce aromatic azo dyes[31]; it can also be applied for the activation of gas phase reactions such as the degradation of volatile organic compounds (e.g., HCHO and CO)[14]. Thus, it can work as a lab-on-a-chip device to assist in developing and understanding new chemical reactions where precise stimulation and monitoring is paramount. In addition to operation in a gas environment or vacuum, it is also possible to use the electrically-driven

metamaterial platform for the activation of reactions in liquid environments (such as ethanol, see Supplementary Section 18). By reciprocity, the metamaterial is also capable of harvesting far-field radiation into localized energy such as hot electrons and heat, which is of interest for applications such as photodetection and thermoelectricity17,43,44. Combining the high sensitivity of tunnel junctions with a compact electric excitation method and the large surface area for hot-electron extraction provided by nanorod metamaterials, the described metamaterial platform merges electronics, plasmonics, photonics, and chemistry for the study and manipulation electrons, plasmons, and photons at the nanoscale.

Methods

Fabrication

Plasmonic nanorod metamaterials were fabricated via Au electrodeposition into nanoporous Al_2O_3 templates on a glass substrate22,24,25. Fabricated metamaterials were then ion-milled (V6000 mill & sputter system, Scientific Vacuum Systems) at an oblique angle of 75º with respect to the normal to the sample surface. Metal-air-metal tunnel junctions were fabricated by using EGaIn (99.99% trace metals basis, Sigma-Aldrich) as a top contact. Because the surface of EGaIn is protected by a native skin of highly conductive Ga_2O_3 (<1 nm in thickness), it provides excellent structural stability to the liquid metal so that EGaIn can deform to match the metamaterial surface but not penetrate into the pores, making it possible to form nanometer-scale air gaps above the nanorod tips. Metal-PLH-metal tunnel junctions (Fig. 3a) were fabricated as follows: firstly, a wet chemical etching method was used to make the surrounding Al_2O_3 matrix lower than the nanorod tips; secondly, the exposed Au nanorods were functionalized with a monolayer of PLH (M_w = 5,000—25,000, Sigma-Aldrich) by self-assembly method to form a ~1.7-nm-thickness dielectric layer; finally, a droplet of EGaIn was added to form the top contact.

Optical characterization

The nanorod metamaterial was mounted vertically on a sample holder, which was then connected to a power supply for the electric excitation and an ammeter to monitor the tunnelling current. A 20X objective (NA = 0.28, Plan Apo SL, Nikon) was used to collect the light emission from the substrate side of the metamaterial, which was then redirected to a spectrometer (Triax 332, Horiba Jobin Yvon) equipped with a charge-coupled device for spectral analysis. All the emission spectra were obtained using the same exposure time of 0.5 s, and then normalized using the spectral response function of the apparatus. The plots in Figs. 3e, 4d, S10 and S11 are the integrated intensity over the measured emission spectra. The long-term and on-off switching stability of the device were also checked (Supplementary Fig. 6).

Numerical simulations

Upon inelastic tunnelling, the emission spectrum from the tunnel junction is defined by a product of the emission spectrum of the tunnelling current source (determined by the Fourier transform of the current fluctuations $C(\omega) \sim \left(1 - \frac{\hbar\omega}{eV}\right)$, where e is the electron charge, V is the applied bias, and $\hbar$ is the Planck's constant28,45), the modal profile of the

metamaterial (determined by the local density of states at the dipole position) and the radiative efficiency of the excited modes in free space7. Numerically, the emission spectrum was found by placing a dipole with a dipole moment determined by $C(w)$ in the tunnelling area and integrating the optical power emitted within the angular range set by the numerical aperture used in the experiment6. The dipole characteristic position was chosen to be $r/\sqrt{2}$ from the nanorod axis (r is the nanorod radius) in the direction of the closest nanorod. The dipole moment was set collinear to the z axis along the direction of the tunnelling current7. For treatment of the full 3D vectorial electromagnetic problem, finite element numerical simulations (COMSOL software package) were employed. To mimic the emission of the dipole in an infinite (in a lateral direction) metamaterial slab, 6×6, 8×8 and 10×10 nanorod arrays were modelled, returning essentially the same results, which confirms the validity of the approach for the infinite array of nanorods. In all the models, the simulation domain was surrounded by perfectly matched layers, ensuring the absence of reflection from its boundaries.

Data availability

All the data supporting this research are presented in full in the results section and supplementary materials. The data that support the plots within this paper and other findings of this study are available from the corresponding author upon reasonable request.

Supplementary Material

Refer to Web version on PubMed Central for supplementary material.

Acknowledgements

References

1. Lambe J, McCarthy SL. Light emission from inelastic electron tunneling. Phys Rev Lett. 1976; 37:923–925.

2. Schneider NL, Schull G, Berndt R. Optical probe of quantum shot-noise reduction at single-atom contact. Phys Rev Lett. 2010; 105:026601. [PubMed: 20867722]

3. Bharadwaj P, Bouhelier A, Novotny L. Electrical excitation of surface plasmons. Phys Rev Lett. 2011; 106:226802. [PubMed: 21702623]

4. Dong ZG, et al. Electrically-excited surface plasmon polaritons with directionality control. ACS Photon. 2015; 2:385–391.

5. Du W, et al. On-chip molecular electronic plasmon sources based on self-assembled monolayer. Nature Photon. 2016; 10:274–280.

6. Kern J, et al. Electrically driven optical antennas. Nature Photon. 2015; 9:582–586.

7. Parzefall M, et al. Antenna-coupled photon emission from hexagonal boron nitride tunnel junctions. Nature Nanotechnol. 2015; 10:1058–1063. [PubMed: 26367108]

8. Bigourdan F, Hugonin J–P, Marquier F, Sauvan C, Greffet J–J. Nanoantenna for electrical generation of surface plasmon polaritons. Phys Rev Lett. 2016; 116:106803. [PubMed: 27015503]

9. Clavero C. Plasmon-induced hot-electron generation at nanoparticle/metal-oxide interfaces for photovoltaic and photocatalytic devices. Nature Photon. 2014; 8:95–103.

10. Brongersma ML, Halas NJ, Nordlander P. Plasmon-induced hot carrier science and technology. Nature Nanotechnol. 2015; 10:25–34. [PubMed: 25559968]

11. Harutyunyan H, et al. Anomalous ultrafast dynamics of hot plasmonic electrons in nanostructures with hot spots. Nature Nanotechnol. 2015; 10:770–774. [PubMed: 26237345]

12. Mubeen S, Lee J, Singh N, Krämer S, Stucky GD, Moskovits M. An autonomous photosynthetic device in which all charge carriers derive from surface plasmons. Nature Nanotechnol. 2013; 8:247–251. [PubMed: 23435280]

13. Mukherjee S, et al. Hot electrons do the impossible: plasmon-induced dissociation of H_2 on Au. Nano Lett. 2013; 13:240–247. [PubMed: 23194158]

14. Christopher P, Xin HL, Linic S. Visible-light-enhanced catalytic oxidation reactions on plasmonic silver nanostructures. Nature Chem. 2011; 3:467–472. [PubMed: 21602862]

15. Kumar A, Kumar S, Rhim W–K, Kim G–H, Nam J–M. Oxidative nanopeeling chemistry-based synthesis and photodynamic and photothermal therapeutic applications of plasmonic core-petal nanostructures. J Am Chem Soc. 2014; 136:16317–16325. [PubMed: 25386786]

16. Zhai YM, et al. Polyvinylpyrrolidone-induced anisotropic growth of gold nanoprisms in a plasmon-driven synthesis. Nature Mater. 2016; 15:889–895. [PubMed: 27376686]

17. Knight MW, Sobhani H, Nordlander P, Halas NJ. Photodetection with active optical antennas. Science. 2011; 332:701–704.

18. Govorov AO, Richardson HH. Generating heat with metal nanoparticles. Nano Today. 2007; 2:30–38.

19. Lock D, Rusimova KR, Pan TL, Palmer RE, Sloan PA. Atomically resolved real-space imaging of hot electron dynamics. Nature Commun. 2015; 6:8365.doi: 10.1038/ncomms9365 [PubMed: 26387703]

20. Albrecht T. Electrochemical tunnelling sensors and their potential applications. Nature Commun. 2012; 3:829.doi: 10.1038/ncomms1791 [PubMed: 22569373]

21. Wang DD, et al. Tuning the tunneling rate and dielectric response of SAM-based junctions via a single polarizable atom. Adv Mater. 2015; 27:6689–6695. [PubMed: 26414779]

22. Kabashin AV, et al. Plasmonic nanorod metamaterials for biosensing. Nature Mater. 2009; 8:867–871. [PubMed: 19820701]

23. Nasir ME, Dickson W, Wurtz GA, Wardley WP, Zayats AV. Hydrogen detected by the naked eye: optical hydrogen gas sensors based on core/shell plasmonic nanorod metamaterials. Adv Mater. 2014; 26:3532–3537. [PubMed: 24643991]

24. Yakovlev VV, et al. Ultrasensitive non-resonant detection of ultrasound with plasmonic metamaterials. Adv Mater. 2013; 25:2351–2356. [PubMed: 23450522]

25. Atkinson R, et al. Anisotropic optical properties of arrays of gold nanorods embedded in alumina. Phys Rev B. 2006; 73:235402.

26. Vasilantonakis N, Nasir ME, Dickson W, Wurtz GA, Zayats AV. Bulk plasmon-polaritons in hyperbolic nanorod metamaterial waveguides. Lasers Photonics Rev. 2015; 9:345–353.

27. Simmons JG. Generalized formula for the electric tunnel effect between similar electrodes separated by a thin insulating film. J Appl Phys. 1963; 34:1793–1803.

28. Johansson P. Light emission from a scanning tunneling microscopy: Fully retarded calculation. Phys Rev B. 1998; 58:10823–10834.

29. Downes A, Taylor ME, Welland ME. Two-sphere model of photon emission from the scanning tunneling microscope. Phy Rev B. 1998; 57:6706–6714.

30. Manjavacas A, Liu JG, Kulkarni V, Nordlander P. Plasmon-induced hot carriers in metallic nanoparticles. ACS Nano. 2014; 8:7630–7638. [PubMed: 24960573]

31. Zhao L–B, et al. Theoretical study of plasmon-enhanced surface catalytic coupling reactions of aromatic amines and nitro compounds. J Phys Chem Lett. 2014; 5:1259–1266. [PubMed: 26274481]

32. Hahn JR, Jang SH, Kim KW, Son SB. Hot carrier-selective chemical reactions on Ag(110). J Chem Phys. 2013; 139:074707. [PubMed: 23968107]

33. Canning NDS, Outka D, Madix RJ. The absorption of oxygen on gold. Surf Sci. 1984; 141:240–254.

34. Huang Y–F, et al. Activation of oxygen on gold and silver nanoparticles assisted by surface plasmon resonances. Angew Chem Int Ed. 2014; 53:2353–2357.

35. Huang Y–F, Zhu H–P, Liu G–K, Ren B, Tian Z–Q. When the signal is not from the original molecule to be detected: chemical transformation of para-aminothiophenol on Ag during the SERS measurement. J Am Chem Soc. 2010; 132:9244–9246. [PubMed: 20527877]

36. Zhao L–B, Liu X–X, Zhang M, Liu Z–F, Wu D–Y, Tian Z–Q. Surface plasmon catalytic aerobic oxidation of aromatic amines in metal/molecule/metal junctions. J Phys Chem C. 2016; 120:944–955.

37. Yalon E, Riess I, Ritter D. Heat dissipation in resistive switching devices: comparison of thermal simulations and experimental results. IEEE Trans Electron Devices. 2014; 61:1137–1144.

38. Davis, ME., Davis, RJ. Fundamentals of Chemical Reaction Engineering. McGraw Hill; New York: 2003.

39. Adleman JR, Boyd DA, Goodwin DG, Psaltis D. Heterogenous catalysis mediated by plasmon heating. Nano Lett. 2009; 9:4417–4423. [PubMed: 19908825]

40. Mukherjee S, et al. Hot-electron-induced dissociation of H_2 on gold nanoparticles supported on SiO_2. J Am Chem Soc. 2014; 136:64–67. [PubMed: 24354540]

41. Sil D, Gilroy KD, Niaux A, Boulesbaa A, Neretine S, Borguet E. Seeing is believing: hot electron based gold nanoplasmonic optical hydrogen sensor. ACS Nano. 2014; 8:7755–7762. [PubMed: 25072929]

42. Pfisterer JHK, Liang YC, Schneider O, Bandarenka AS. Direct instrumental identification of catalytically active surface sites. Nature. 2017; 549:74–77. [PubMed: 28880284]

43. Chalabi H, Schoen D, Brongersma ML. Hot-electron photodetection with a plasmonic nanostripe antenna. Nano Lett. 2014; 14:1374–1380. [PubMed: 24502677]

44. Aradhya SV, Venkataraman L. Single-molecule junctions beyond electronic transport. Nature Nanotechnol. 2013; 8:399–410. [PubMed: 23736215]

45. Rendell RW, Scalapino DJ. Surface plasmons confined by microstructures on tunnel junctions. Phys Rev B. 1981; 24:3276–3294.
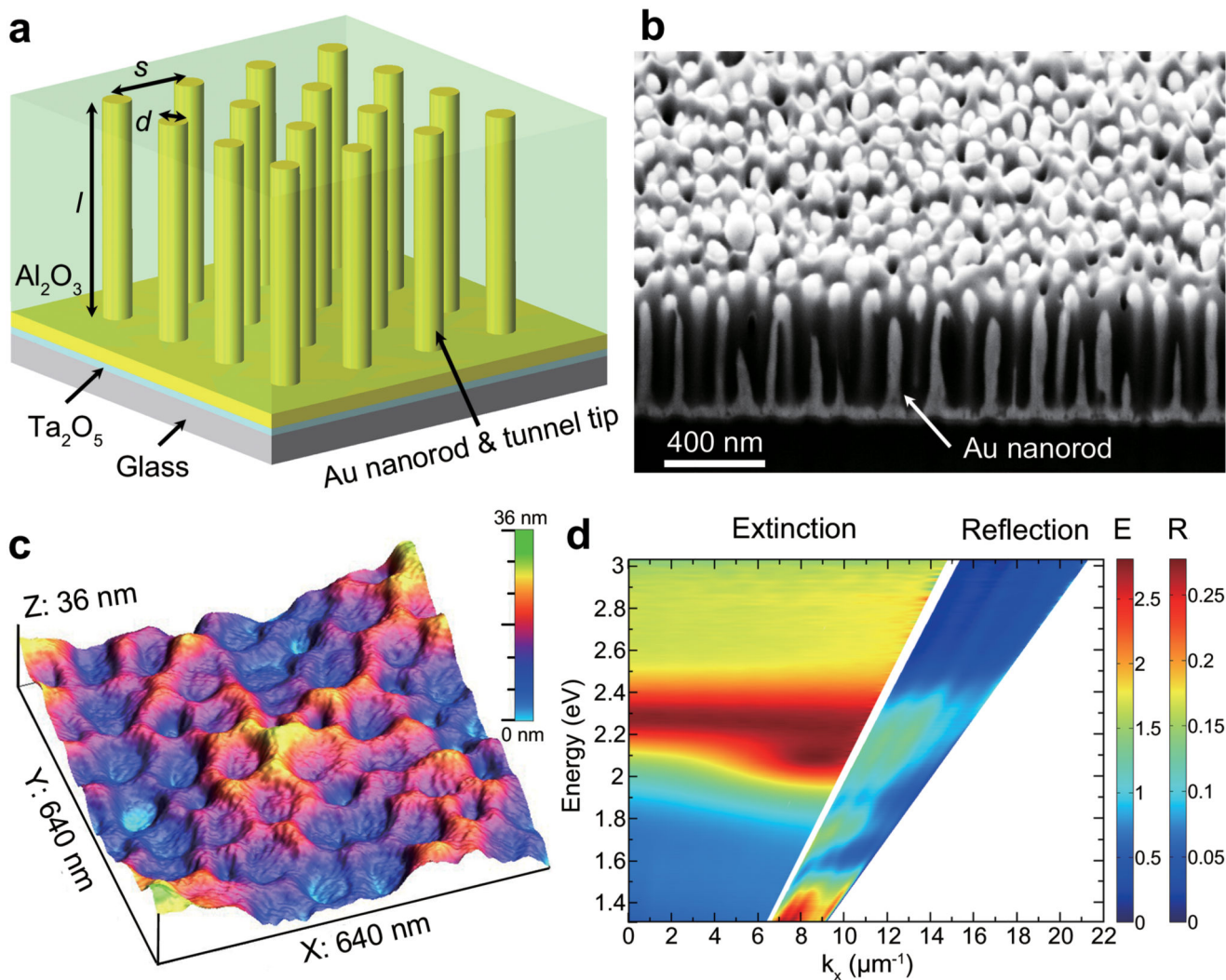
Figure 1. Structural and optical properties of plasmonic nanorod metamaterials.
a, Schematic diagram of the nanorod metamaterial, where d and l represent the diameter and length of the nanorods, respectively, and s is the separation between the nanorods. **b**, Cross-sectional view of a metamaterial showing Au nanorods embedded in a porous Al_2O_3 template. **c**, Surface morphology of an ion-milled metamaterial analysed by atomic force microscopy. The dips are the tips of Au nanorods surrounded by Al_2O_3. **d**, Experimental dispersion of extinction (for the angles below total internal reflection) and reflection (for the angles above total internal reflection) of the metamaterial for TM-polarized illumination.
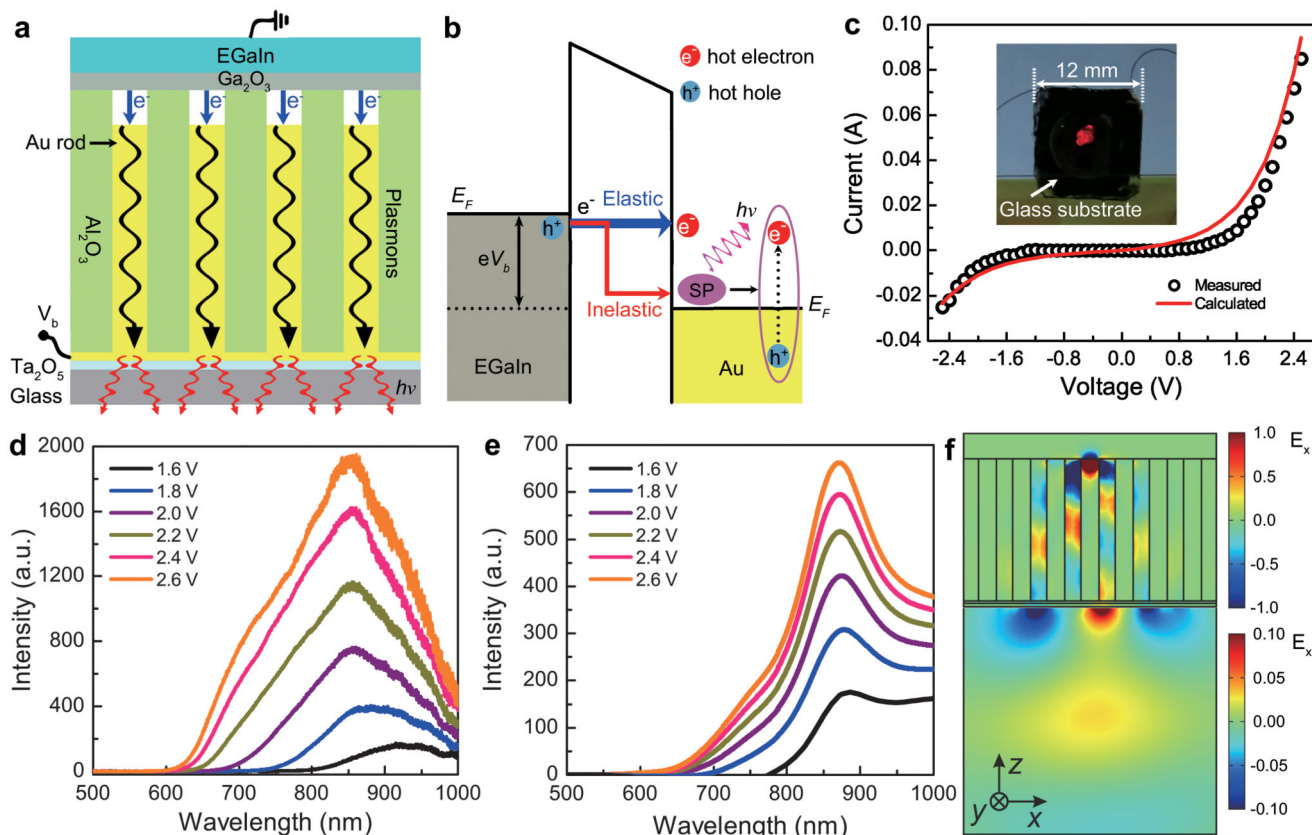
Figure 2. Electrically-driven nanorod metamaterial based on metal-air-metal tunnel junctions.
a,b, Schematics of the device configuration (**a**) and the tunnelling processes (**b**). When a bias is applied between the EGaIn and Au nanorods, electrons tunnel across the junctions from occupied states in EGaIn to unoccupied states in Au nanorods. The majority of electrons tunnel elastically to form hot electrons in the Au nanorod tips; the inelastically tunnelling electrons excite surface plasmons in the metamaterial, which can then decay non-radiatively via the excitation of hot carriers or radiatively into photons from the substrate side of the metamaterial. **c**, Experimentally measured and theoretically calculated current–voltage curves for a device fabricated using the metamaterial shown in Fig. 1. Inset, photograph of the device with an applied bias of $V_b = 2.5$ V. **d,e**, Measured (**d**) and simulated (**e**) emission spectra of the device as a function of the applied forward bias. **f**, Simulated near-field map of the metamaterial plasmonic mode excited via tunnelling and the subsequent radiation of the optical signal into the far field.
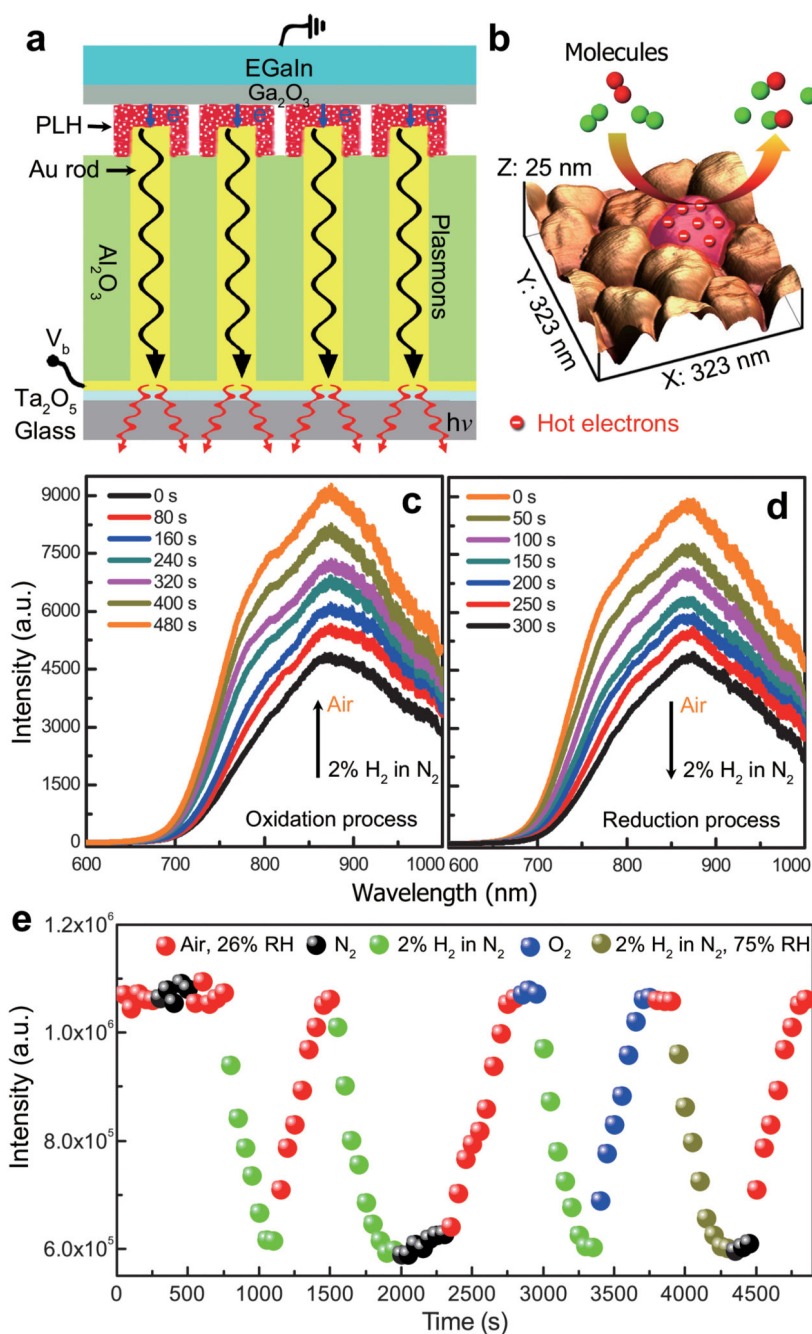
Figure 3. Electrically-driven nanorod metamaterial with reactive tunnel junctions.
a, Schematic diagram of the device configuration based on metal-polymer-metal tunnel junctions. The Al_2O_3 matrix was first chemically etched in order to expose the Au nanorod tips. The nanorod tips were then functionalized with a monolayer of poly-L-histidine (PLH) which works both as a tunnel barrier and a reactant. **b**, Surface morphology of an etched metamaterial with the exposed nanorod tips. **c,d**, The evolution of the emission spectra of the metamaterial ($V_b = 2.5$ V) when the cell atmosphere was switched from N_2 with 2% H_2 to air (**c**) and from air to N_2 with 2% H_2 (**d**). **e**, Integrated emission power from the

metamaterial measured when the cell atmosphere was dynamically changed between air, N_2, 2% H_2 in N_2, O_2, and 2% H_2 in N_2 with 75% RH.
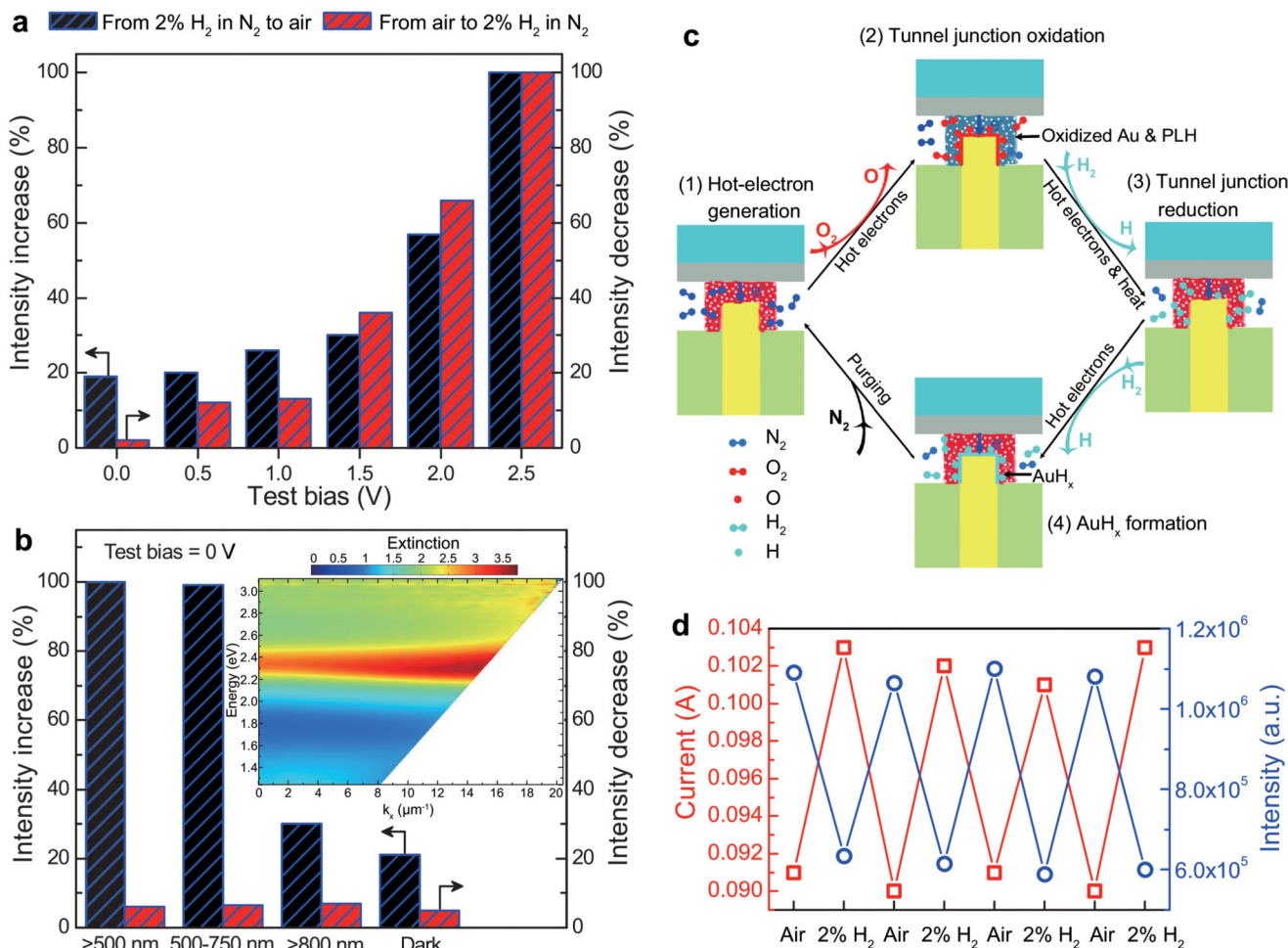
Figure 4. Electro-photo-chemistry in nanoscale tunnel junctions.
a, Changes of the emission intensity from the device during 10-min period for different test biases without external illumination, plotted from Supplementary Fig. 10. **b**, Changes of the emission intensity from the device during 10-min period under various external illumination conditions without applied bias, plotted from Supplementary Fig. 11. Inset, experimental dispersion of extinction of the metamaterial for TM-polarized illumination. **c**, Schematics of the mechanism for the chemical reactions in the reactive tunnel junction. **d**, Tunnelling current (red hollow squares) and emission power (blue hollow circles) measured when the cell atmosphere was cycled betweent air and N_2 with 2% H_2 under V_b = 2.5 V bias.